Unraveling the dissociation of dimethyl sulfoxide following absorption at 193 nm

David A. Blank, Simon W. North,[a] Domenico Stranges,[b] Arthur G. Suits, and Yuan T. Lee[c]
Chemical Sciences Division, Lawrence Berkeley Laboratory, University of California, Berkeley, California 94720 and Department of Chemistry, University of California, Berkeley, California 94720

(Received 3 September 1996; accepted 3 October 1996)

We have studied the photodissociation of dimethyl sulfoxide, DMSO-h_6 and DMSO-d_6, at 193 nm using the technique of photofragment translational spectroscopy with a tunable vacuum ultraviolet product probe provided by undulator radiation on the Chemical Dynamics Beamline at the Advanced Light Source. In contrast to previous investigations we have found the dissociation to proceed via a stepwise mechanism involving multiple reaction channels. The primary dissociation, S–C bond cleavage to eliminate a methyl radical, was found to have two competing channels with distinct translational energy distributions. The translational energy distribution for the major primary dissociation channel suggests that it proceeds in a statistical manner on the ground electronic surface following internal conversion. In competition with this channel is a primary dissociation that exhibits a translational energy distribution suggestive of dissociation on an excited electronic surface with most of the available energy partitioned into translational and electronic degrees of freedom. Secondary decomposition of the CD_3SO intermediate was found to proceed exclusively via C–S bond cleavage, $CD_3SO \rightarrow CD_3+SO$. However, secondary decomposition of the CH_3SO intermediate was found to exhibit competition between $CH_3SO \rightarrow CH_3+SO$ and $CH_3SO \rightarrow CH_2SO+H$. The dissociation to CH_3 and SO was the major secondary decomposition channel with the translational energy distribution indicating a barrier to recombination of >8 kcal/mol. While a minor hydrogen atom elimination channel was found to play a role in secondary decomposition of CH_3SO intermediates, no analogous secondary C–D bond cleavage was detected from the CD_3SO intermediates indicating the importance of tunneling in the secondary decomposition of CH_3SO. © *1997 American Institute of Physics.* [S0021-9606(97)01702-9]

I. INTRODUCTION

When a molecule with two equivalent chemical bonds is excited above the threshold for dissociation of both bonds, how the rupture of the two bonds are temporally coupled becomes a salient question. For discussions of the temporal correlation of the dissociating bonds we adopt here the convenient experimental definitions of concerted and stepwise mechanisms, where concerted refers to cleavage of both bonds prior to rotation of the intermediate, and stepwise refers to cleavage of the bonds in two distinct steps with the lifetime of the intermediate exceeding its rotational period.[1] Recently the question of a concerted versus stepwise dissociation has been addressed in our laboratory for such three-body dissociation processes as azomethane[2] and acetone,[3] where the technique of photofragment translational spectroscopy (PTS) was demonstrated to be particularly adept at resolving the dissociation dynamics. Characterization of such correlations between dissociating bonds is difficult using time-resolved techniques for cases where the first step is predissociative rather than direct owing to the uncertainty in the determination of time zero.[4] Here we have continued the investigation of this class of photodissociation using PTS to study the UV dissociation of dimethyl sulfoxide, DMSO. At 193 nm there is sufficient energy to break both of the C–S bonds in DMSO. The dissociation can proceed in either a concerted [Reaction (1)] or stepwise [Reaction (2)] manner[5,6]

$$CH_3SOCH_3 \rightarrow CH_3+SO+CH_3, \quad \Delta H = 103 \text{ kcal/mol}, \tag{1}$$

$$CH_3SOCH_3 \rightarrow CH_3SO+CH_3, \quad \Delta H = 51 \text{ kcal/mol}, \tag{2a}$$

$$CH_3SO \rightarrow CH_3+SO, \quad \Delta H = 52 \text{ kcal/mol}. \tag{2b}$$

In addition to dissociation to two methyl radicals and sulfur monoxide, the following dissociation channels are also thermodynamically accessible at 193 nm[5,6]

$$CH_3SOCH_3 \rightarrow CH_3SO+CH_3 \rightarrow CH_2SO+H+CH_3, \quad \Delta H = 106 \text{ kcal/mol}, \tag{3}$$

$$CH_3SOCH_3 \rightarrow C_2H_6+SO, \quad \Delta H = 13 \text{ kcal/mol}, \tag{4}$$

$$CH_3SOCH_3 \rightarrow CH_2SO+CH_4, \quad \Delta H = 2 \text{ kcal/mol}. \tag{5}$$

The room temperature UV absorption spectrum of DMSO was recorded by Gollnick and Stracke.[7] The absorption at 188 nm was attributed to a $(\pi^* \leftarrow \pi)$ transition on the SO moiety and the absorption at 205 nm to either a $(\sigma^* \leftarrow n)$ or $(d \leftarrow n)$ transition. The only published investigations of

[a]Current address: Chemistry Department, Brookhaven National Laboratory, Brookhaven, New York, 11973-5000.
[b]Permanent address: Dipartimento di Chimica, Università ''La Sapienza,'' 00185, Rome, Italy.
[c]Permanent address: Institute of Atomic and Molecular Science, Academica Sinica, Taipei 10764, Taiwan.

the gas phase UV photodissociation of DMSO have been reported by Chen *et al.* dissociating at 193 nm.[8] They used LIF (laser induced fluorescence) on both the (A-X) and (B-X) transitions to probe the the SO products, and 2+1 REMPI (resonance enhanced multiphoton ionization) to probe the methyl radical products. They found the SO vibrational distribution to be inverted, peaked at $v=2$. They also assigned rotational temperatures for the SO products at 750–1450 K and reported the SO quantum yield at 1.02 ± 0.12. The results of the 2+1 REMPI measurements made on the methyl radical products found them to be internally cold with only 1.9 kcal/mol of internal energy on average in each methyl. Based on their measurements of the partitioning of the available energy the authors concluded that the dissociation of DMSO at 193 nm proceeds along a single reaction path to produce $SO+2CH_3$ in a concerted three-body elimination, reaction 1. The inverted SO vibrational distribution was attributed to an elongated S–O bond length in the electronically excited DMSO. Since concerted elimination processes represent the exception for three-body dissociations, the suggestion that DMSO dissociates in a concerted manner at 193 nm presents it as a particularly interesting dynamical system for investigation.

In this study we have used PTS with VUV product ionization to investigate the dissociation dynamics of DMSO-h_6 and DMSO-d_6 following absorption at 193 nm. We have observed direct evidence that the dissociation to form SO and two methyl radicals proceeds via a stepwise mechanism. Our SO photoionization measurements agree with the internal energy measured for the SO product by Chen *et al.*, however, our measured translational energy distributions suggest a much larger fraction of the available energy is partitioned into internal excitation of the methyl radical products than reported from the 2+1 REMPI results. In contrast to the conclusions of Chen *et al.* we have found the dissociation to be considerably more complex involving multiple decomposition channels. We have identified competing dissociation channels in both the primary dissociation involving C–S bond cleavage to eliminate a methyl radical as well as the secondary decomposition of the sufonyl intermediate. This study represents one of the first applications of vacuum ultraviolet (VUV) undulator radiation as a photofragment probe in PTS experiments and demonstrates this technique to be a powerful new tool for investigations in chemical dynamics.

II. EXPERIMENT

For detection of all neutral photofragments except hydrogen atoms, the experiments were carried out on the Chemical Dynamics Beamline at the Advanced Light Source (ALS) at Lawrence Berkeley National Laboratory.[9] The apparatus will be described in detail in a forthcoming publication.[10,11] The design is based on an apparatus currently used in our laboratory and described elsewhere,[12] with the most significant difference being the use of tunable VUV undulator radiation from the ALS for product ionization in place of electron impact ionization. A complete description of the undulator radiation at the Chemical Dynamics Beamline can be found in Ref. 11. The light is continuously tunable from 8–50 eV with a bandwidth of 2.5% providing an average of 5×10^{15} photons/sec at the fundamental energy and substantial power in the higher harmonics. The undulator radiation is passed through a harmonic filter that consists of a gas cell containing 30 torr of noble gas. For undulator radiation at energies below the I.P. for the noble gas the filter is transparent. However, above the I.P. of the noble gas the filter provides a $>10^4$ suppression of the light. By selecting a gas with an I.P. between the fundamental and the second harmonic energy of the undulator radiation, the higher order harmonics from the undulator are efficiently filtered from the VUV beam. The undulator radiation is then focused to 150 $\times$200 micrometers at the point of intersection with the dissociation products.

A continuous molecular beam of either DMSO-h_6 or DMSO-d_6, $<1\%$ in He, was generated by bubbling 40–60 torr of He through a room temperature liquid sample and expanding the resulting mixture through a 0.25 mm stainless steel nozzle into a source chamber maintained at 1×10^{-4} torr. The nozzle was heated to 80 °C to inhibit cluster formation and the resulting molecular beam typically had a r.m.s. velocity of 1080 m/s with FWHM of 15%. After being skimmed twice the molecular beam was intersected at 90° by the output of a Lambda Physik LPX200 excimer laser operating on the ArF transition (193.3 nm) with laser fluence ranging 1–500 mJ/cm^2. The molecular beam was rotatable about the axis of the dissociation laser, with the dissociation laser and detector axes fixed mutually perpendicular. Neutral photofragments, which recoiled out of the molecular beam, traveled 15.1 cm where they were photoionized by the undulator radiation, mass selected with a quadrupole mass filter, and counted as a function of time using a Daly ion counter.[13]

For detection of hydrogen atoms a similar apparatus was used with modifications designed to increase sensitivity for m/e 1 photofragments which have been discussed previously.[14] In this configuration a pulsed molecular beam of $<1\%$ DMSO-h_6 in He, the dissociation laser, and the detector axis are all fixed mutually perpendicular. The dissociation laser intersects the unskimmed molecular beam 5 mm above the pulsed nozzle exit. Neutral photofragments that recoil at 90° from the molecular beam pass through two defining apertures and travel 37.0 cm where they are ionized by electron impact, mass selected, and counted as a function of time in the same manner as described above.

Center of mass translational energy distributions, $P(E_T)$s, for the neutral photofragments were obtained from the time of flight spectra, TOF, using the forward convolution technique.[12,15] The forward convolution technique involves convolution of an initial $P(E_T)$ over the instrument response function to simulate the TOF spectra. The simulated TOF spectra are then compared with the raw data and the $P(E_T)$ is iteratively adjusted until the best fit to the raw data is obtained.

DMSO-h_6, 99%, and DMSO-d_6, 99.9% isotopic purity, were obtained from Aldrich and used without further purification.

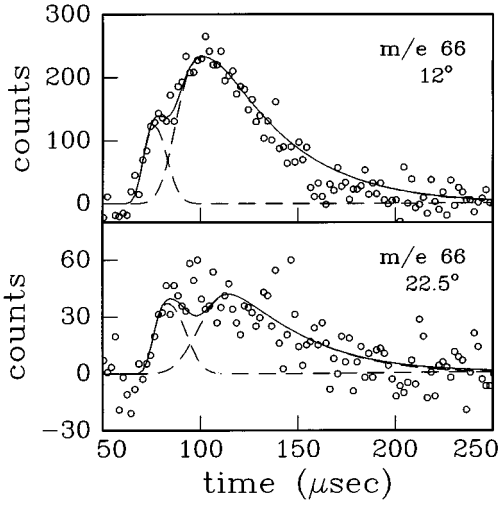

FIG. 1. TOF spectra for m/e 66 (CD_3SO^+) at source angles of 12° and 22.5°. The forward convolution fit contains two contributions representing the fast and slow channels for reaction (2a) and fit with the $P(E_T)$'s in Fig. 2.

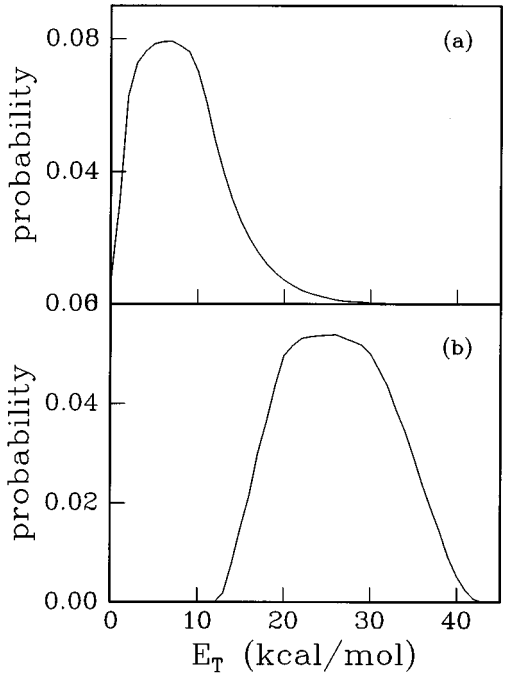

FIG. 2. (a) c.m. translational energy distribution used to fit the slow contribution in the m/e 66 (CD_3SO^+) TOF spectra (Fig. 1). (b) c.m. translational energy distribution used to fit the fast contribution in the m/e 66 (CD_3SO^+) TOF spectra (Fig. 1).

III. RESULTS

For all of the TOF spectra presented the open circles represent the data, the dashed lines are single channel contributions to the forward convolution fit, and the solid line is the overall fit to the data.

A. DMSO-d_6

The TOF spectra for m/e 66 (CD_3SO^+) at source angles of 12° and 22.5° are shown in Fig. 1. Each spectrum is the result of 2×10^6 laser shots with the undulator radiation set at 11.0 eV. Not only do these spectra directly identify CD_3SO as a primary dissociation product, reaction (2a), but the spectra suggest that there is more than one dissociation channel resulting in CD_3SO photoproducts. The spectrum at 12° exhibits a clear shoulder ~80 μsec and the spectrum has been fitted with two separate contributions. The presence of the contribution at earlier flight times is confirmed in the 22.5° spectrum. The c.m. translational energy distribution for each of the two contributions are shown in Fig. 2. The primary dissociation channel that produces slow photofragments [Fig. 2(a)], is peaked around 8 kcal/mol and has a tail that extends beyond 30 kcal/mol. The primary dissociation channel that produces fast photofragments [Fig. 2(b)] is peaked at 26 kcal/mol and extends to 42 kcal/mol. Additional evidence for two channels leading to CD_3SO can be seen in Fig. 3, the TOF spectrum for m/e 64 (CD_2SO^+) at 12°, which was taken under the same photoionization conditions as the m/e 66 spectra. Different dissociation channels leading to CD_3SO products demonstrate different dissociative ionization patterns as a result of the distinct internal energy distributions in the CD_3SO products. Figure 3 has been fitted with the $P(E_T)$'s in Fig. 2 and it is clear that while the primary dissociation channel that produces slow photofragments is still evident with dissociative ionization slightly favoring the translationally slower, and therefore internally warmer, fragments, the primary dissociation channel that produces fast photofragments is not observed at the CD_2SO mass. The failure to detect any of the primary channel that produces fast photofragments at m/e 64, demonstrates that the CD_3SO fragments from that channel are vibrationally much cooler than the primary channel that produces slow photofragments, with an internal energy distribution distinct from the slow photofragment dissociation channel.

The TOF spectra for m/e 18 (CD_3^+) at source angles of 20, 35, and 50° are shown in Fig. 4 and were taken with the undulator radiation set at 12.0 eV and without the use of the harmonic filter. The spectra have been fitted with three contributions. The contribution at the earliest flight times is fit-

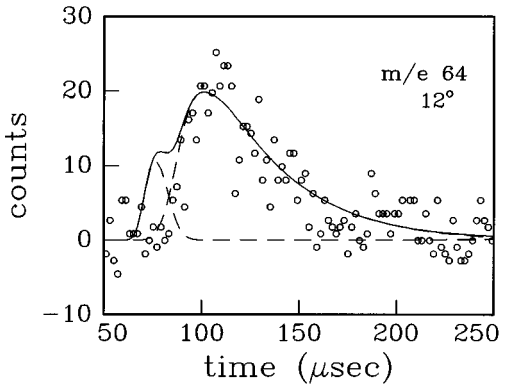

FIG. 3. TOF spectrum for m/e 64 (CD_2SO^+) at a source angle of 12°. The fit shown is from the two $P(E_T)$'s in Fig. 2 with the same fitting ratio used to fit the m/e 66 (CD_3SO^+) spectra in Fig. 1. Note absence of the fast feature in the experimental data.

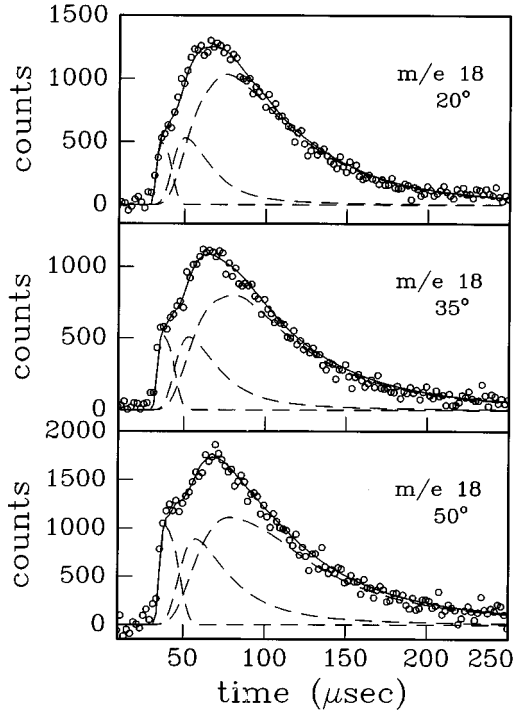

FIG. 4. TOF spectra for m/e 18 (CD_3^+) at source angles of 20°, 35°, and 50°. The forward convolution fit has three components. The fastest component, peaked ~40 μsec is fit with the $P(E_T)$ in Fig. 2(b) and represents the fast channel for reaction (2a). The slowest and broadest component, peaked ~80 μsec, is fitted with the $P(E_T)$ in Fig. 5(a) and represents the slow channel for reaction (2a). The middle contribution, peaked ~55 μsec, is fitted with the secondary $P(E_T)$ in Fig. 5(b) and represents products from reaction (2b).

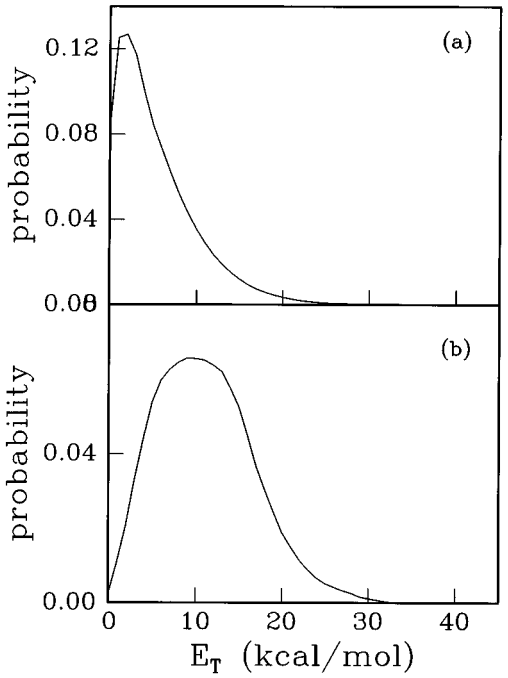

FIG. 5. (a) Primary c.m. translation energy distribution used to fit the slowest contribution to the m/e 18 (CD_3^+) TOF spectra in Fig. 4, slow channel for reaction (2a). (b) Secondary c.m. translation energy distribution for reaction (2b) used to fit the middle contribution to the m/e 18 (CD_3^+) TOF spectra in Fig. 4 and the dominant contribution to the m/e 48 (SO^+) TOF spectra in Fig. 7.

ted with the $P(E_T)$ for the primary channel which produced fast photofragments observed at m/e 66, Fig. 2(b), confirming the fast methyl photofragments as the momentum matched dissociation partners of the fast CD_3SO fragments. The remaining two contributions are the broad contribution peaked at ~80 μsec that are the methyl products from the slow photofragment primary dissociation channel, reaction (2a); and the contribution peaked ~55 μsec representing methyl products that result from secondary decomposition of those primary CD_3SO fragments produced with sufficient internal energy to undergo secondary dissociation, reaction (2b). The $P(E_T)$ for the primary dissociation channel that results in slow photofragments is shown in Fig. 5(a). It is peaked near zero with an exponential decrease extending beyond 30 kcal/mol. Since methyl radical products do not undergo secondary decomposition, the $P(E_T)$ in Fig. 5(a) represents the complete $P(E_T)$ for the slow photofragment primary dissociation channel. Figure 6 shows the $P(E_T)$ from Fig. 5(a), along with the $P(E_T)$ from Fig. 2(a), which is the $P(E_T)$ for the slow photofragment primary CD_3SO dissociation products that survive. The primary $P(E_T)$ for CD_3SO intermediates that undergo secondary decomposition is the difference between Figs. 5(a) and 2(a), shown as the crossed-hatched region in Fig. 6. For a discussion of the truncation in the primary $P(E_T)$ for the surviving CD_3SO photofragments, see Sec. IV B. The $P(E_T)$ for the secondary decomposition of CD_3SO intermediates [reaction (2b)], produced in the slow photofragment primary dissociation is shown in Fig. 5(b). It is peaked at 8 kcal/mol and extends to 32 kcal/mol.

TOF spectra for m/e 48 (SO^+) at source angles of 25, 40, and 50° are shown in Fig. 7 and were taken under the same photoionization conditions as the m/e 18 spectra. The fit to the TOF consists predominantly of the signal from the sec-

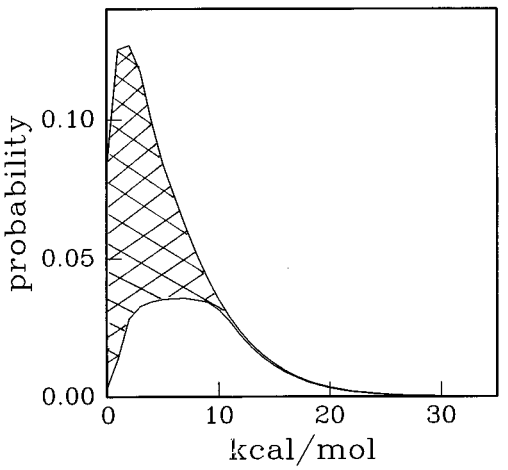

FIG. 6. The c.m. translational energy distribution from Fig. 2(a) overlayed on the c.m. translation energy distribution from Fig. 5(a). The area with the cross-hatches is the difference between Figs. 5(a) and 2(a) and represents the primary c.m. translation energy distribution for sulfonyl intermediates that undergo secondary C–S bond cleavage.

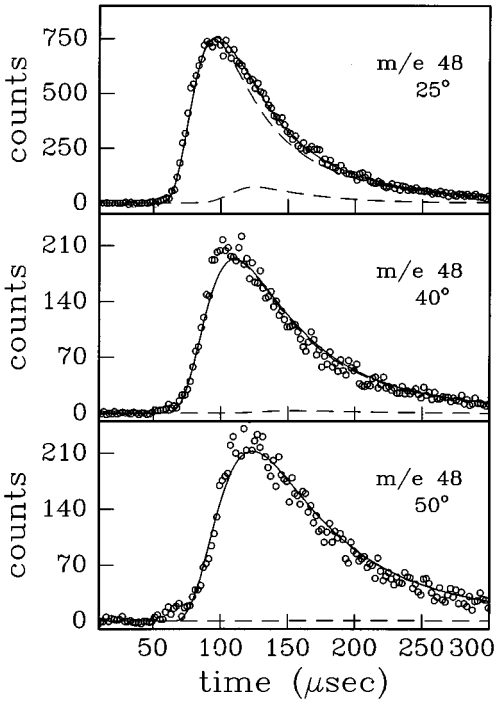

FIG. 7. TOF spectra for m/e 48 (SO^+) from dissociation of DMSO-d_6 at source angles of 25°, 40°, and 50°. The dominant contribution to the forward convolution fit is the result of reaction (2b) and is fitted with the $P(E_T)$ in Fig. 5(b). The small contribution to the fit at 25°, peaked ~125 μsec, is from dissociative ionization of CD_3SO photoproducts.

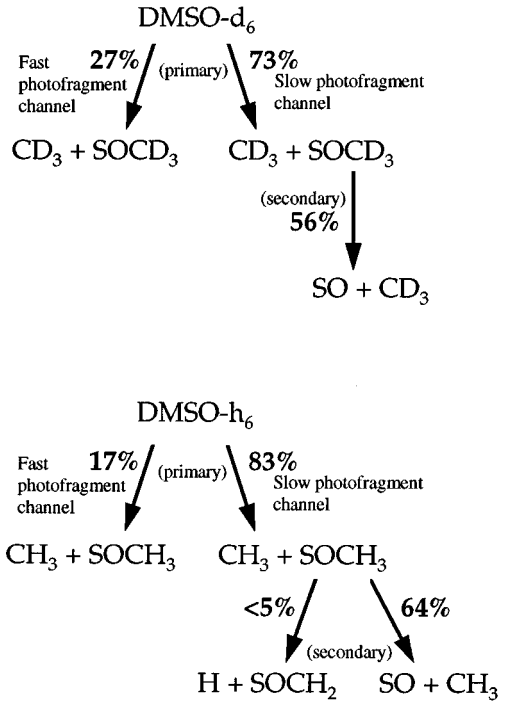

FIG. 8. Branching ratios for the dissociation of DMSO-d_6 and DMSO-h_6 at 193 nm. Determination of the values is discussed in the text. The error in the values is estimated to be <10%.

ondary decomposition of the CD_3SO intermediates produced in the slow photofragment primary dissociation channel. There is a small contribution to the m/e 48 TOF spectra from dissociative ionization of CD_3SO intermediates, which is peaked at ~130 μsec and is most evident in the 25° spectrum. As mentioned above for the secondary CD_3 products, the primary $P(E_T)$ for CD_3SO intermediates that undergo secondary decomposition is represented by the difference between Figs. 5(a) and 2(a), (see Fig. 6). The m/e 48 (SO^+) spectra were fitted using the secondary $P(E_T)$ in Fig. 5(b), confirming the secondary methyl contribution in the m/e 18 TOF spectra to be the momentum matched partner of the SO. Although the fits to the secondary decomposition of the CD_3SO intermediates at m/e 18 (CD_3^+) and m/e 48 (SO^+) were not sensitive to the precise shape of the secondary angular distribution, the fits did require that the secondary angular distribution maintain forward/backward symmetry.

Branching ratios. The branching ratios are depicted in Fig. 8. The branching ratios were obtained from the fitting ratios of the three contributions to the m/e 18 (CD_3^+) TOF spectra. We, therefore, assumed that under the experimental photoionization conditions the photoionization cross-section for the methyl radical products was independent of their internal energy. All kinematic considerations are accounted for in the fitting procedure. The ratio of the three channels used to obtain the best fit to the m/e 18 spectra was 19 (primary, fast photofragments):52 (primary, slow photofragments):29 (secondary). This yields a ratio of 27:73 for the fast photofragment primary dissociation channel to the slow photofragment primary dissociation channel. With the secondary dissociation proceeding exclusively from the slow photofragment primary dissociation, the fitting ratios indicate that 56% of the CD_3SO fragments produced in the slow photofragment primary dissociation undergo secondary decomposition. The best fits to the CD_3SO spectra, m/e 66, were obtained with a ratio of 44 (primary, fast photofragments):56 (primary, slow photofragments). This ratio of the fast primary CD_3SO products to the surviving slow primary CD_3SO intermediates is consistent with the measured ratios for the m/e 18 spectra. With 56% of the slow photofragment primary channel undergoing secondary decomposition the result is a ratio of 45:55 for the fast photofragment primary channel to the surviving slow secondary CD_3SO products, which is consistent with the fitting ratio for the m/e 66 TOF spectra. The majority of the error in the branching ratios obtained in this fashion results from the ability to adjust the fitting ratios while maintaining a reasonable fit to all of the TOF data. We estimate this error to be <10%.

B. DMSO-h_6

We were not able to observe TOF spectra for m/e 63 (CH_3SO^+). The inability to directly detect the CH_3SO intermediate is the result of a number of experimental factors. As will be shown, in comparison with the CD_3SO intermediates, a greater percentage of the CH_3SO intermediates produced in the slow photofragment primary dissociation undergo secondary decomposition. In addition, the fast photofragment primary dissociation is less prevalent in the case of

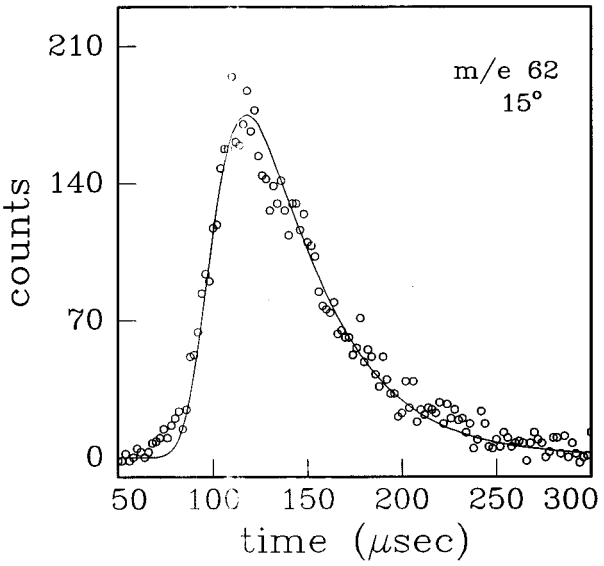

FIG. 9. TOF spectrum for m/e 62 (CH_2SO^+) at a source angle of 15°. The forward convolution fit is from the primary and secondary $P(E_T)$'s in Figs. 10(a) and 10(b) according to reaction (3).

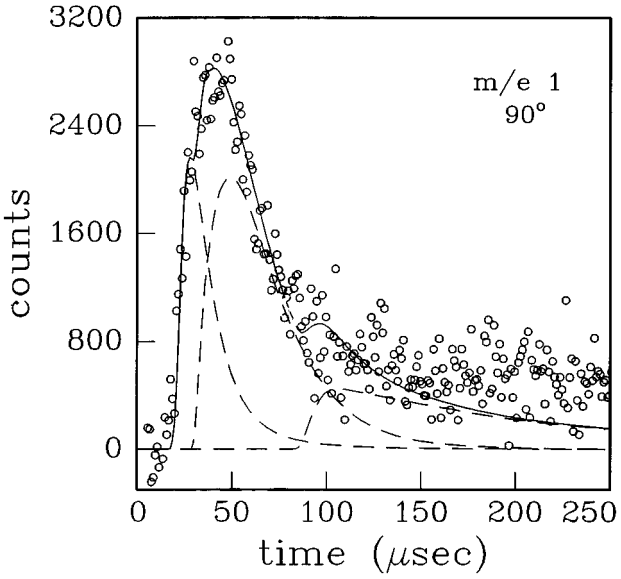

FIG. 10. TOF spectrum for m/e 1 (H^+) with the detector, molecular beam, and dissociation laser mutually perpendicular. The forward convolution fit contains three contributions. The fastest contribution, peaked ~40 μsec, is a two-photon dissociation involving C–S bond cleavage followed by secondary photodissociation of the methyl radical products. The slowest contribution, peaked ~105 μsec; is from dissociative ionization of methyl radical products. The middle contribution, peaked ~60 μsec is fit with the primary and secondary $P(E_T)$'s in Figs. 10(a) and 10(b) according to reaction (3).

DMSO-h_6. Although this accounts for a reduction of ~30% in the yield of CH_3SO intermediates in the dissociation, the most substantial reduction in signal results from the necessity to increase the resolution of the quadrupole mass filter to permit sufficient discrimination between m/e 62 and m/e 63. The increased resolution is accompanied by a severe reduction in transmission of the quadrupole. The low signal at m/e 66 (CD_3SO^+) from the the CD_3SO intermediate was likely the result of preferential photodissociation rather than photoionization, and the additional reductions in signal for the CH_3SO rendered it unobservable under the experimental conditions.

Although we were not able to detect any signal at m/e 63 (CH_3SO^+), we observed a substantial signal at m/e 62. The TOF spectrum for m/e 62 (CH_2SO^+) at a source angle of 15° is shown in Fig. 9. The spectrum was taken with the undulator radiation set at 12 eV without the harmonic filter. The signal at m/e 62 can be attributed to either dissociative ionization of CH_3SO intermediates or to secondary decomposition of the CH_3SO intermediates involving hydrogen atom elimination [reaction (3)]. Direct evidence for reaction (3) is shown in Fig. 10, the TOF spectrum for m/e 1 (H^+). The fit to the m/e 1 TOF spectrum contains three contributions. The slow contribution, peaked at 110 μsec, is the contribution from dissociatively ionized methyl radical products scattered to 90°. The contribution at early times, peaked at 30 μsec, exhibits a near quadratic dependence on the dissociation laser fluence and has been fitted as a two-photon dissociation with the first photon yielding methyl radical products and the second photon dissociating the methyl radicals to methylene and hydrogen atoms. The $P(E_T)$ for methyl radical photodissociation at 193 nm has been previously determined in this laboratory[14] and was used in the fitting for the secondary step in the two-photon dissociation. The remaining middle feature, peaked at 50 μsec had a linear dependence on the laser power and was fitted assuming a stepwise mechanism for reaction (3). The translational energy distributions for the primary, $CH_3SOCH_3 \rightarrow CH_3 + SOCH_3$, and the secondary dissociation, $SOCH_3 \rightarrow SOCH_2 + H$, are shown in Fig. 11. The $P(E_T)$'s in Fig. 11 were also used to fit the TOF spectrum for m/e 62 in Fig. 9, providing strong evidence that the m/e 62 TOF signal is the result of reaction (3). The primary $P(E_T)$ is peaked at 6 kcal/mol and exponentially declines beyond 30 kcal/mol, and the secondary $P(E_T)$ is peaked at 4 kcal/mol and extends to 18 kcal/mol.

TOF spectra for m/e 15 (CH_3^+) at source angles of 20° and 35° are shown in Fig. 12. The undulator radiation was set at 11 eV and the harmonic filter was used with argon.[11] The fitting is analogous to the m/e 18 (CD_3^+) spectra described above with the same three individual contributions. Owing to reasons discussed above, we were not able to observe spectra for the CH_3SO fragment and we have therefore assumed the $P(E_T)$ in Fig. 2(b) from the fast photofragment primary dissociation channel of DMSO-d_6 in fitting the fast contribution peaked ~30 μsec. The remaining two contributions are the slow photofragment primary dissociation, the slowest and broadest contribution peaked around 70 μsec, and subsequent secondary decomposition of the CH_3SO intermediate, reaction (2b), peaked ~40 μs. The $P(E_T)$ for fitting the slow photofragment primary dissociation, reaction (2a), is shown in Fig. 13(a) and is identical to the analogous $P(E_T)$ for the deuterated case in Fig. 5(a). The $P(E_T)$ used to fit the secondary decomposition, Reaction (2b), is shown

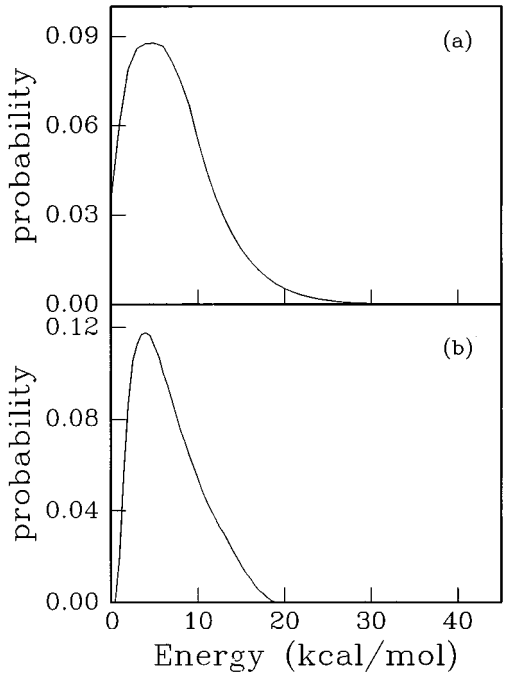

FIG. 11. (a) Primary c.m. translation energy distribution used to fit the m/e 62 (CH_2SO^+) TOF spectrum in Fig. 9 and the middle contribution to the m/e 1 (H^+) TOF spectrum in Fig. 10, reaction (3). (b) Secondary c.m. translation energy distribution for reaction (3) used to fit the m/e 62 (CH_2SO^+) TOF spectrum in Fig. 9 and the middle contribution to the m/e 1 (H^+) TOF spectrum in Fig. 10.

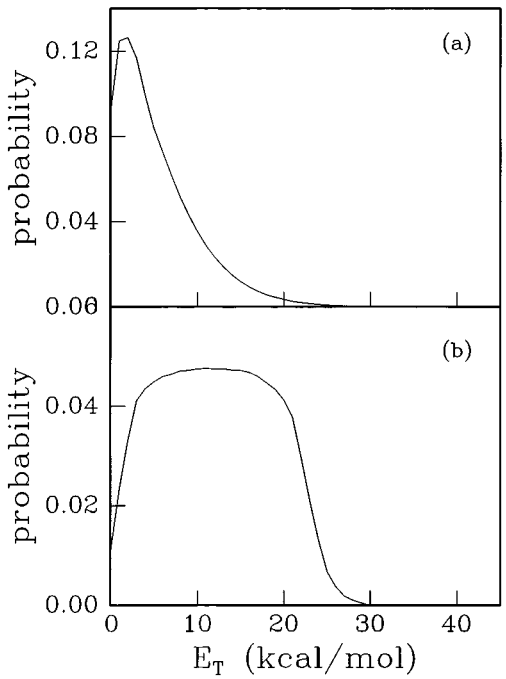

FIG. 13. (a) Primary c.m. translation energy distribution used to fit the slowest contribution to the m/e 15 (CH_3^+) TOF spectra in Fig. 12, slow channel for reaction (2a). (b) Secondary c.m. translation energy distribution for reaction (2b) used to fit the middle contribution to the m/e 15 (CH_3^+) TOF spectra in Fig. 12 and the dominant contribution to the m/e 48 (SO^+) TOF spectra in Fig. 14.

in Fig. 13(b). The TOF spectra for the momentum matched secondary SO fragments, m/e 48 (SO^+), at source angles of 20, 30, and 45°, are shown in Fig. 14. The dominant contribution is from decomposition of the CH_3SO intermediates,

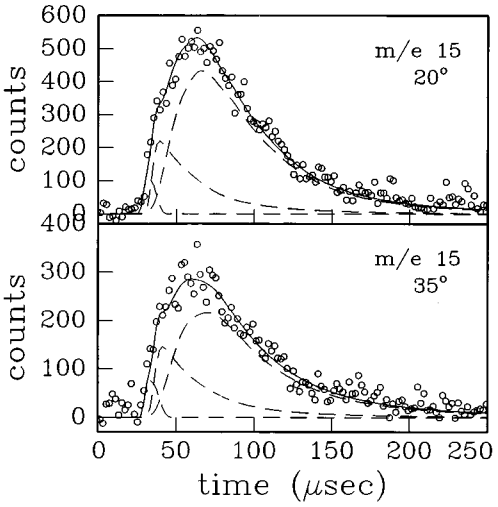

FIG. 12. TOF spectra for m/e 15 (CH_3^+) at source angles of 20° and 35°. The forward convolution fit has three components. The fastest component, peaked ~40 μsec; is fit with the $P(E_T)$ in Fig. 2(b) and represents the fast channel for reaction (2a). The slowest and broadest component, peaked ~75 μsec is fit with the $P(E_T)$ in Fig. 13(a) and represents the slow channel for reaction (2a). The middle contribution, peaked ~45 μsec; is fit with the secondary $P(E_T)$ in Fig. 13(b) and represents products from reaction (2b).

Reaction (2b), fitted with the secondary $P(E_T)$ in Fig. 13(b). At 20 and 30° there is a small contribution on the slow side from dissociative ionization of CH_3SO photofragments. Although the secondary $P(E_T)$ is very similar to the analogous $P(E_T)$ for the deuterated dissociation [Fig. 5(b)], it is slightly broader. As with the fits to the DMSO-d_6 data, the secondary angular distribution was not sensitive to the exact shape of the distribution. However, the fits did require that forward/backward symmetry be maintained.

Photoionization spectrum of the SO product. Figure 15 shows the relative intensity of the TOF signal at m/e 48 and a source angle of 20° as a function of the photoionization energy from 8.25 eV to 11.0 eV. For this measurement, in addition to the rare gas harmonic filter, the undulator radiation passed through a 3 mm thick MgF_2 window to further reduce background from residual high energy photons above the transmission cutoff for MgF_2 of about 11.2 eV. The energy distribution of the undulator radiation had a FWHM of 2.5%. From Fig. 15 the ionization onset for the SO products is ~9.5 eV. Taking into consideration the bandwidth of the undulator radiation, this corresponds to an onset of ~9.8 eV. The vertical I.P. for sulfur monoxide is 10.32 ± 0.02 eV.[17] The difference between the ionization onset for the SO product and the vertical I.P. reflects an internal energy content in the SO of 0.50 ± 0.15 eV.

Branching ratios. The branching ratios are depicted in Fig. 8. The ratio between the fast photofragment primary channel, slow photofragment primary channel, and secondary C–S bond cleavage was obtained from the fits to the m/e

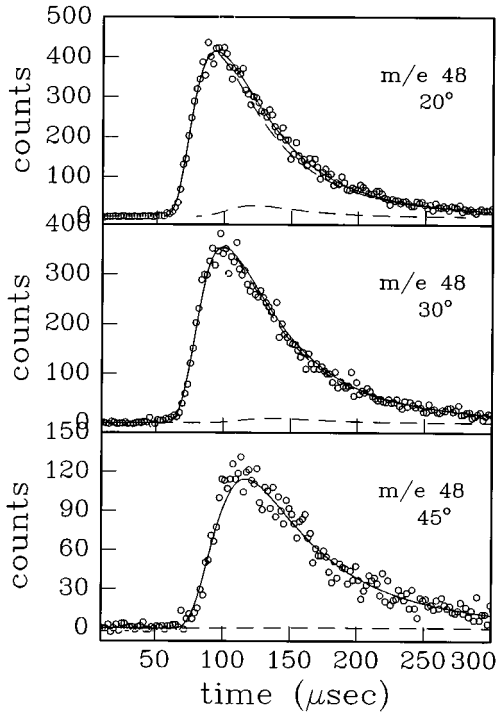

FIG. 14. TOF spectra for m/e 48 (SO^+) from dissociation of DMSO-h_6 at source angles of 20°, 30°, and 45°. The dominant contribution to the forward convolution fit is the result of reaction (2b) and is fit with the $P(E_T)$ in Fig. 13(b). The small contribution to the fit at 20°, peaked ~125 μsec, is from dissociative ionization of CH_3SO photoproducts.

15 (CH_3^+) spectra. The best fit to the data resulted from a ratio of 11:54:35, respectively, indicating 65% of the CH_3SO intermediates produced in the slow primary step undergo secondary decomposition. The error in the ratios between the contributions in the m/e 15 fits is analogous to the case of DMSO-d_6, <10%. In order to estimate the percentage of the secondary hydrogen elimination [reaction (3)], we must compare the signal intensity of the m/e 62 and m/e 15 TOF spectra. Since there is no current information on the photoionization cross-section for CH_2SO at 12 eV we make the assumption that the photoionization cross sections of CH_3 at 11.0 eV and CH_2SO at 12.0 eV are equal and we estimate the contribution of reaction 3 at <5% overall.

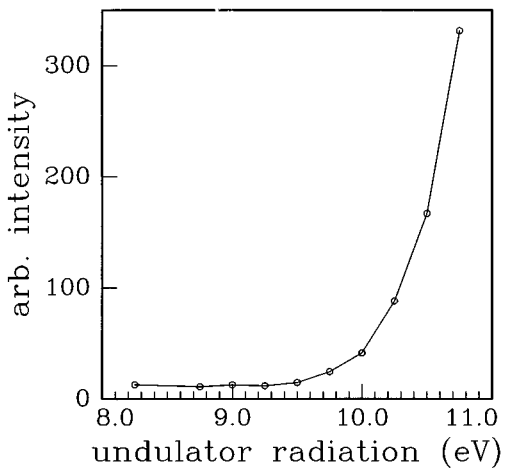

FIG. 15. Photoionization spectrum for m/e 48 (SO^+) photofragments from DMSO-h_6 at a source angle of 20° for undulator radiation energies of 8.25–10.75 eV. The VUV had a roughly Gaussian shape in energy with FWHM of 0.5 eV.

IV. DISCUSSION

A. Primary dissociation [reaction (2a)]

Detection of the CD_3SO product at m/e 66 (see Fig. 1), provides strong evidence that the dissociation to sulfur monoxide and two methyl radicals does not exclusively proceed via a three-body process. The TOF spectrum for m/e 66 at 12° in Fig. 1 exhibits a shoulder on the fast side suggesting two contributions to the spectrum, a contribution peaked at 80 μsec, and a slower broad contribution peaked at 100 μsec. The existence of two separate contributions is confirmed by the differing dissociative ionization at m/e 64 (CD_2SO^+) (see Fig. 3), indicating the production of two different m/e 66 photoproducts with distinct vibrational energy distributions. As discussed above we were not able to detect the CH_3SO photoproducts due to experimental limitations (see Sec III B). However, the fits to the TOF spectra at m/e 15 confirm the analogous fast and slow primary dissociations in the case of DMSO-h_6.

Fast photofragment primary dissociation. The $P(E_T)$ for the fast photofragment primary dissociation [reaction (2a)] shown in Fig. 2(b) is peaked at 24 kcal/mol and extends to a maximum of 42±5 kcal/mol. Assuming the maximum in the $P(E_T)$ reflects the production of vibrationally/rotationally cold products, and neglecting the internal energy of the DMSO reactant,[18] the maximum in the $P(E_T)$ represents the available energy following photodissociation at 193 nm (148 kcal/mol). Given an available energy of 42±5 kcal/mol and using $\Delta H_f(\mathrm{DMSO}) = -31.4$ kcal/mol and $\Delta H_f(\mathrm{CH_3}) = 34.8$ kcal/mol (see Ref. 5) the result is $\Delta H_f(\mathrm{CH_3SO}) = 40 \pm 5$ kcal/mol. Comparison of this value to the value obtained from group additivity of $\Delta H_f(\mathrm{CH_3SO}) = -15$ kcal/mol (Ref. 6) suggests that the fast primary dissociation might result in the production of an excited electronic state of CH_3SO, which lies ~55 kcal/mol above the ground electronic state. The lack of dissociative ionization of the fast m/e 66 (CD_3SO^+) product to m/e 64 (CD_2SO^+), as compared with the slow photofragment primary dissociation (see Figs. 1 and 2), indicates the fast CD_3SO product is vibrationally much cooler than the slow CD_3SO product. This also indicates that the electronically excited CD_3SO products must undergo radiative relaxation during the ~30 μsec collisionless flight to the detector since nonradiative relaxation would result in vibrational excitation which is not evident in the dissociative ionization at m/e 64 (CD_2SO^+). The large fraction of available energy partitioned into translation, $\langle E_{\mathrm{trans}} \rangle = 26$ kcal/mol, and the fact that the distribution is peaked at 24 kcal/mol suggests either direct dissociation on a repulsive electronic surface or electronic predissociation on a surface with a large barrier to recombination.

From the absorption spectrum of Gollnick and Stracke[7] the dominant absorption at 193 nm should be a ($\pi^* \leftarrow \pi$) transition on the SO moiety. The fast photofragment primary dissociation may then be the result of electronic predissociation involving a repulsive electronic surface. Comparison of TOF spectra taken at m/e 18 (CD_3^+) and 35° with the dissociation laser polarized at −45°, 0°, 45°, and 90° with respect to the detector axis demonstrated no difference in the overall TOF spectra. Assuming an isotropic angular distribution for the slow photofragment primary dissociation, a reasonable assumption for a statistical dissociation on the ground electronic surface (see Sec. IV A), no change in the relative intensity of the fast photofragment channel to slow photofragment channel contributions in the TOF with polarization suggests a near isotropic angular distribution for the fast photofragment primary dissociation. A first order approximation of the dipole moment for a ($\pi^* \leftarrow \pi$) transition within C_{2v} symmetry places the dipole moment in the plane of the molecule along the S═O bond. Based on a ground state CSC bond angle of 96.4° (Ref. 7) the angle between the dipole and the C–S bond is 48.2°, leading to an anisotropy parameter[19] of $\beta=0.34$ in the limit of a prompt dissociation. While in the excited state the CSC bond angle might be expected to increase, this would only lead to a decrease in the limiting value of β. In addition, any rotational averaging of the reactant molecule prior to dissociation will also serve to decrease the value of β. Our data for m/e 18 at various laser polarization angles is not sufficient to distinguish within this small range of values for β, $0<\beta<0.3$. Therefore, our measurement of an angular distribution for the fast photofragment primary dissociation channel, which appears nearly isotropic in the laboratory frame, is consistent with electronic predissociation from the π^* surface on even a very rapid timescale owing to our lack of sensitivity to the degree to which the distribution is anisotropic.

Slow photofragment primary dissociation. The $P(E_T)$ for the slow photofragments primary dissociation [reaction (2a)] is shown in Figs. 5(a) and 13(a) for DMSO-d_6 and DMSO-h_6, respectively. Within experimental error, Figs. 5(a) and 13(a) are the same. Note that the $P(E_T)$ in Fig. 2(a) determined from the slow m/e 66 (CD_3SO^+) photoproducts differs from Figs. 5(a) and 13(a) on the low energy side. As will be discussed below, a significant fraction of the slow CD_3SO products undergo secondary decomposition and therefore the $P(E_T)$ in Fig. 2(a) represents only those CD_3SO photofragments that survive. The $P(E_T)$ in Figs. 5(a) and 13(a) were determined from the methyl radical product that does not secondarily decompose, and, therefore, represents the complete $P(E_T)$ for the slow photofragment primary dissociation.

The $P(E_T)$ for the slow photofragment primary dissociation [Figs. 5(a) or 13(a)], is peaked at 2 kcal/mol and decreases exponentially out beyond 30 kcal/mol. Translational energy distributions of this type, peaked near zero with an exponentially decreasing tail, are characteristic of statistical dissociation on the ground electronic surface involving little or no recombination barrier. From the endothermicity of the primary C–S bond cleavage, $D_0(CH_3\text{-}SOCH_3)=51$ kcal/mol,[5,6] the available energy following absorption at 193 nm (148 kcal/mol) is 97 kcal/mol. In the case of a statistical translational energy distribution, the extremely low probability for formation of products with a translational energy release greater than half of the available energy severely limits our sensitivity to the $P(E_T)$ above 50 kcal/mol. For comparison, Fig. 16 shows a prior distribution for dissociation of a rotationally cold molecule into two polyatomic fragments of four and six atoms each within the rigid rotor, harmonic oscillator, and spherical top approximations, and given 97 kcal/mol of available energy.[20] The prior distribution represents a completely statistical prediction against which the experimentally determined distribution may be compared. From Fig. 16 it is clear that the measured $P(E_T)$ (dashed line) is in excellent agreement with the prior translational energy distribution (solid line). Our results indicate that in the case of the slow photofragment primary dissociation the initial electronic excitation is followed by internal conversion to the ground electronic surface and C–S bond cleavage to produce two open shell molecules with little or no barrier to recombination.

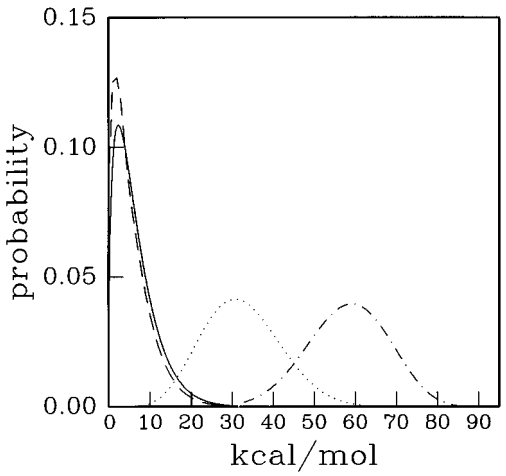

FIG. 16. Calculated prior distributions for dissociation of a rotationally cold reactant into 4 and 6 atom fragments within the rigid rotor, harmonic oscillator, and spherical top approximations with 97 kcal/mol of available energy. The solid line is the calculated translational energy distribution. The dotted line is the internal energy distribution of the four atom product. The dotted-dashed-dotted line is the internal energy distribution of the six atom product. The dashed line is the primary $P(E_T)$ for the slow channel of reaction (2a) from Figs. 5(a) and 13(a).

B. Secondary decomposition of the sulfonyl intermediate, CD_3SO/CH_3SO

Following the primary dissociation [reaction (2a)] the sulfonyl intermediates containing sufficient internal energy will undergo secondary decomposition. We found no evidence for the secondary dissociation of products produced in the fast photofragment primary dissociation. The fast photofragment primary dissociation (see Sec. IV A) results in the production of electronically excited sulfonyl radicals with a substantial fraction of the available energy appearing in translation. The predominant partitioning of the

available energy into translational and electronic degrees of freedom and the lack of dissociative ionization of the fast m/e 66 (CD_3SO^+) photoproduct at m/e 64 (CD_2SO^+) are consistent with the persistence of the sulfonyl radicals produced in the fast photofragment primary dissociation.

In contrast with the fast photofragment primary dissociation, sulfonyl intermediates produced in the slow photofragment primary dissociation should contain ample internal energy to undergo secondary dissociation. As discussed in Sec. IV A, the slow photofragment primary dissociation is a statistical, near prior, dissociation on the ground electronic surface. Figure 6 shows the overall slow photofragment primary channel $P(E_T)$, with the $P(E_T)$ for the surviving CD_3SO fragments overlaid. The distributions are the same above ~20 kcal/mol but at lower translational energy, and thus higher internal energy of the products, the distribution for the surviving CD_3SO fragments begins to fall off. The difference between the two distributions, the cross-hatched area in Fig. 6, represents the CH_3SO/CD_3SO fragments that undergo secondary decomposition. The gradual decline in the $P(E_T)$ for the surviving CD_3SO fragments toward lower translational energy reflects the broad internal energy distribution of the methyl partner fragment. In the case of atomic elimination a given translational energy release reflects a well-defined internal energy in the polyatomic partner fragment and the result is an abrupt truncation of the $P(E_T)$ for the surviving polyatomic fragment.[21] In this case the broad internal energy distribution in the methyl partner fragment allows a broad distribution of internal energy in the CD_3SO fragments for a given translational energy release yielding a gradual truncation of the $P(E_T)$.

The onset of the truncation in the $P(E_T)$ for surviving CD_3SO photofragments occurs at the point where internally cold methyl radicals are produced along with sulfonyl radicals with internal energy equal to the height of the barrier to secondary sulfonyl radical decomposition. The recombination barrier for secondary C–S bond cleavage is >8 kcal/mol (see the next section). Adding the recombination barrier to the C–S bond energy for the sulfonyl radical of ~52 kcal/mol the barrier to secondary C–S bond cleavage is ~60 kcal/mol. The onset of the truncation in the primary $P(E_T)$ should therefore occur at ~37 kcal/mol since the available energy following primary C–S bond cleavage is ~97 kcal/mol. With the onset of the truncation reflecting production of internally cold methyl radicals, the portion of the $P(E_T)$ measured for the surviving sulfonyl intermediates below ~37 kcal/mol directly reflects the internal energy distribution of methyl radicals produced with surviving sulfonyl radicals. As can be seen in Fig. 2(a) the $P(E_T)$ lies almost entirely below 37 kcal/mol.

Using the prior model, in Fig. 16, to predict the internal exitation in the sulfonyl intermediate following the slow photofragment primary dissociation, $\langle E_{\text{int}}(CD_3SO/CH_3SO)\rangle_{\text{prior}}=58$ kcal/mol with the distribution extending beyond 90 kcal/mol. Both cleavage of the C–S bond [reaction (2b)], and cleavage of the C–H/C–D bond, [reaction (3)], are, therefore, thermodynamically accessible pathways for secondary decomposition of the sulfonyl intermediate.

Secondary decomposition of the CD_3SO/CH_3SO intermediate: C–S bond cleavage. Cleavage of the C–S bond [reaction (2b)] was the dominant secondary dissociation channel for the CH_3SO intermediates, and the only secondary decomposition pathway detected for the CD_3SO intermediates. As discussed above in Sec. IV B the difference between the the overall $P(E_T)$ for the slow photofragment primary dissociation and the $P(E_T)$ for surviving sulfonyl intermediates (the cross-hatched area in Fig. 6), represents the primary $P(E_T)$ for the CD_3SO/CD_3SO fragments that undergo secondary decomposition. In Fig. 6 the difference between the two distributions represents 55% of the total distribution, consistent with 56±10% secondary decomposition determined from the CD_3 TOF spectra fitting ratios. For reasons discussed in Sec. III B we were unable to directly detect the surviving CH_3SO photofragments, however, in the fitting we assumed the primary $P(E_T)$ for CH_3SO intermediates that secondarily dissociate to be the same as that for the CD_3SO photofragments. From the fitting ratios in the CH_3 TOF spectra we find that 64±10% of the CH_3SO intermediates undergo secondary decomposition. This corresponds to a quantum yield for the SO of 0.6±0.1 compared to the quantum yield reported by Chen *et al.* for SO of 1.02±0.12.[8]

The $P(E_T)$ determined for secondary C–S bond cleavage is shown in Fig. 5(b) for CD_3SO and in Fig. 13(b) for CH_3SO. The distributions are very similar, however, the $P(E_T)$ for CH_3SO decomposition is slightly broader and a little flatter at the top of the distribution. This difference is likely the result of competing C–H bond cleavage in the case of CH_3SO decomposition, which is discussed in the following section. In addition, stiffer modes in the CH_3 product, as compared to the CD_3 product, might result in less vibrational excitation of the CH_3 product and, therefore, a slightly faster $P(E_T)$ for the CH_3SO decomposition. The translational energy distributions [Figs. 5(b) and 13(b)] are peaked at ~8 kcal/mol suggesting a barrier to recombination of >8 kcal/mol. If one considers a dissociation model for simple bond rupture over an exit barrier where the available energy is partitioned in an impulsive fashion up to the height of the barrier to recombination and statistically above the barrier,[3] then the maximum probability in the translational energy distribution will reflect the barrier to recombination. The success of this model for different chemical systems with widely differing available energies has shown that the barrier to recombination is predominantly responsible for energy partitioned into translation even when the available energy greatly exceeds the barrier height.[4] The limiting case results if all the potential energy of the recombination barrier appears in translation. Since it is possible for some portion of that potential energy to evolve into internal degrees of freedom as the dissociation proceeds, our measured maximum in the $P(E_T)$ represents a lower limit to the recombination barrier. In the case of both the deuterated and nondeuterated DMSO the fits to the data were not sensitive to the exact shape of the secondary angular distribution, however, the fits did require that the secondary angular distribution maintain

forward/backward symmetry, demonstrating rotational averaging of the CD_3SO intermediate prior to secondary C–S bond dissociation and providing direct evidence that reaction (2) proceeds via a stepwise mechanism.[23] In the case of a concerted three-body elimination we would have measured a strong correlation between the primary and secondary recoil velocity vectors.[2]

Our measurement of the SO internal energy found 11.5 $\pm$3.5 kcal/mol on average, which agrees well with the more accurate measurement of Chen *et al.* who found an average of 8.9 kcal/mol with the vibrational distribution peaked at $v=2$.[8] From our results we conclude that SO products result from a stepwise dissociation [reaction (2)] with a statistical primary dissociation followed by secondary decomposition over a recombination barrier of $>$8 kcal/mol. This suggests that the dynamical partitioning of available energy into SO internal degrees of freedom results from strong exit channel effects in the secondary decomposition of the sulfonyl intermediate.

From the measured branching ratios we find a quantum yield for CH_3/CD_3 of 1.4$\pm$0.1. This is in excellent agreement with recent diode absorption gain measurements made by Rudolph and co-workers who determined a quantum yield of 1.4$\pm$0.1 for CD_3 from the dissociation of DMSO-d_6 at 193 nm.[22] In addition, Rudolph and co-workers determined the fraction of nascent methyl radical products formed in the vibrational ground state. Their measurements suggest an internal energy content of the CD_3 products in excess of the REMPI measurements of Chen *et al.*[8] and below the internal energy content which had been previously determined for CD_3 products in the dissociation of acetone-d_6 at 193 nm.[24] For comparison we can make a qualitative estimate of the vibrational energy in the methyl radical products based on our overall picture of the dissociation of DMSO-d_6 at 193 nm. The fast primary dissociation accounts for 19% of the total methyl radical yield. Using the soft fragment impulsive model[4] with 42 kcal/mol of available energy (see Sec. IV A) we estimate $\langle E_{\rm int}(CH_3/CD_3)\rangle\sim$4 kcal/mol for the fast photofragment primary dissociation. For the slow photofragment primary dissociation, which accounts for 52% of the total methyl radical yield, we use the prior model (see Sec. IV A) to estimate $\langle E_{\rm int}(CH_3/CD_3)\rangle\sim$32 kcal/mol. The remaining 29% of the methyl radical products are the result of secondary decomposition of sulfonyl intermediates. As discussed earlier in this section, the forward barrier to C–S bond cleavage in the sulfonyl radical intermediates is $\sim$60 kcal/mol. For sulfonyl radicals produced in the slow photofragment primary dissociation we can again use the prior model as an estimate of the internal energy distribution (see Fig. 16). Truncating the distribution below 60 kcal/mol to represent only those sulfonyl radicals that undergo secondary decomposition yields $\langle CH_3SO/CD_3SO\rangle_{\rm int}\sim$67 kcal/mol. With $D_0(CH_3-SO)\sim$52 kcal/mol,[5,6] $\langle E_T\rangle$=11 kcal/mol for secondary C–S bond cleavage, and $\langle E_{\rm int}(SO)\rangle\sim$9 kcal/mol (see Ref. 8) suggests very little energy remaining in internal energy of the methyl radical. Based on these estimates, overall the methyl radical products will contain $\sim$17 kcal/mol of internal energy each on average. While we acknowledge the severity of the approximations made in this estimation, it clearly suggests a larger internal energy content in the methyl products than the REMPI measurements of Chen *et al.*

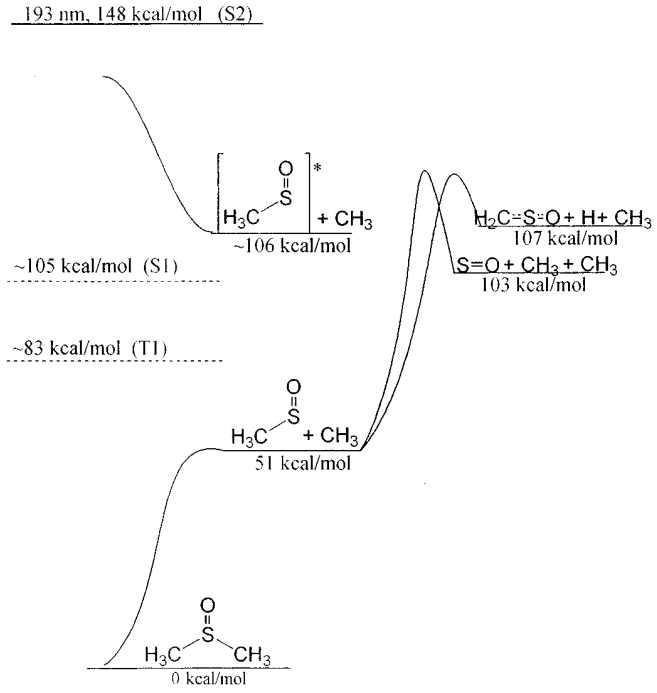

FIG. 17. A summary of the dissociation channels that we observed for DMSO following absorption at 193 nm. Thermodynamic values are from Refs. 5 and 6 and estimations for the energy of $S1$, $T1$, and $S2$ are from Ref. 7. Relative contributions of each channel are shown in Fig. 8.

Secondary decomposition of the CH_3SO intermediate: C–H bond cleavage. The primary and secondary translational energy distributions for reaction (3) that were determined from the fitting of the m/e 62 (CH_2SO^+) and m/e 1 (H^+) TOF spectra are shown in Fig. 11. Our inability to detect any evidence of C–D bond cleavage in the CD_3SO intermediates suggests that secondary C–H bond cleavage involves tunneling through the dissociation barrier. The secondary $P(E_T)$ [Fig. 11(b)], is peaked at $\sim$4 kcal/mol. Since the C–H bond cleavage appears to involve tunneling, the barrier to recombination should be slightly higher than the 4 kcal/mol reflected by the maximum in the $P(E_T)$. This places the barrier to secondary dissociation for reaction (2b) and reaction (3) in very close proximity of one another (see Fig. 17). Figure 11(a) shows the $P(E_T)$ for the primary C–S bond cleavage, and although it is similar to the overall slow photofragment primary $P(E_T)$ in Fig. 13(a), it is missing a portion of the low energy side. In contrast, the primary $P(E_T)$ for sulfonyl intermediates that undergo secondary C–S bond cleavage (the region cross-hatched in Fig. 6) is missing the high energy side in comparison to the overall slow photofragment primary $P(E_T)$. This indicates that CH_3SO intermediates that go on to break a C–H bond are internally cooler, and therefore translationally warmer, on average compared with those that break the C–S bond. The resulting overall picture for the secondary decomposition of the CH_3SO intermediates shows that the fraction of CH_3SO

intermediates with substantial internal energy above the barriers to secondary dissociation result almost exclusively in C–S bond cleavage. However, a small portion of the CH_3SO intermediates with internal energy near the dissociation barriers are able to break the C–H bond with tunneling playing an important role.

V. CONCLUSION

We have used the technique of photofragment translational spectroscopy with VUV synchrotron radiation for product ionization to investigate the photodissociation of DMSO-h_6 and DMSO-d_6 at 193 nm. A picture of the overall dissociation including all of the observed dissociation channels and the estimated barriers is shown in Fig. 17. In contradiction to previous studies we found direct evidence that dissociation to sulfur monoxide and two methyl radicals occurs via a stepwise dissociation on the ground electronic surface. In addition we also found competing dissociation channels in both the primary and secondary steps. A small fraction of the primary dissociation results in a very large translation energy release and appears to involve dissociation on an excited electronic surface to form the methyl radical and an electronically excited state of the sulfonyl radical. With the majority of the available energy partitioned into electronic and translational degrees of freedom the sulfonyl radicals from the fast photofragment primary dissociation lack sufficient internal energy to undergo secondary decomposition. The majority of the primary dissociation occurs following an initial ($\pi^* \leftarrow \pi$) excitation and internal conversion to the ground electronic surface. Primary C–S bond cleavage then proceeds over little or no barrier resulting in a statistical, near prior, partitioning of the available energy. In the case of DMSO-d_6 all of the CD_3SO intermediates with sufficient internal energy to overcome the barrier to C–S bond cleavage, 56% of the $SOCD_3$ produced in the slow photofragment primary dissociation, dissociate via reaction (2b). In the case of DMSO-h_6 those sulfonyl intermediates with internal energy well above the barrier to secondary C–S bond cleavage go on to dissociate via reaction (2b), however, a small fraction of CH_3SO intermediates with internal energy near the dissociation barriers are able to break the C–H bond with tunneling playing a significant role.

ACKNOWLEDGMENTS

The authors would like to thank R. N. Rudolph for providing a preprint of the results of the diode absorption gain experiments. The authors would like to thank Dr. G. E. Hall for many helpful discussions. This work was supported by the Director, Office of Energy Research, Office of Basic Energy Sciences, Chemical Sciences Division of the U.S. Department of Energy under contract No. DE-AC03-76SF0009. The experiments were conducted at the Advanced Light Source, Lawrence Berkeley National Laboratory, which is supported by the same source.

[1] C. E. M. Strauss and P. L. Houston, J. Phys. Chem. **94**, 8751 (1990).
[2] S. W. North, C. A. Longfellow, and Y. T. Lee, J. Chem. Phys. **99**, 4423 (1993).
[3] S. W. North, D. A. Blank, J. D. Gezelter, C. A. Longfellow, and Y. T. Lee, J. Chem. Phys. **102**, 4447 (1995).
[4] S. W. North, Ph.D. thesis, University of California, Berkeley, 1995.
[5] The heat of formation for DMSO was taken from Phys. Chem. Ref. Data **17**, (1988) Suppl. No. 1. The heats of formation for SO, CH_3, H, C_2H_6, and CH_4 were taken from *Handbook of Chemistry and Physics* (CRC, Boca Raton, 1995).
[6] The heat of formation for CH_3SO and CH_2SO were based on group additivity from S. W. Benson, Chem. Rev. **78**, 23 (1978).
[7] K. Gollnick and H. U. Stracke, Pure Appl. Chem. **33**, 217 (1973).
[8] X. Chen, F. Asmar, H. Wang, and B. R. Weiner, J. Phys. Chem. **95**, 6415 (1991); X. Chen, H. Wang, B. R. Weiner, M. Hawley, and H. H. Nelson, *ibid*. **97**, 12269 (1993).
[9] M. Koike, P. A. Heimann, A. H. Kung, T. Namioka, R. DiGennaro, B. Gee, N. Yu, Nuclear Instruments and Methods in Physics Research A **347**, **282** (1994); P. A. Heimann, M. Koike, C. W. Hsu, M. Evans, C. Y. Ng, D. Blank, X. M. Yang, C. Flaim, A. G. Suits, and Y. T. Lee, SPIE Proceedings **2856** (1996).
[10] X. Yang, D. A. Blank, J. Lin, P. A. Heimann, A. M. Wodtke, A. Suits, and Y. T. Lee (unpublished).
[11] A. G. Suits, P. Heimann, X. Yang, M. Evans, C. Hsu, K. Lu, and Y. T. Lee, Rev. Sci. Instrum. **66**, 4841 (1995).
[12] A. M. Wodtke and Y. T. Lee, J. Phys. Chem. **89**, 4744 (1985).
[13] Y. T. Lee, J. D. McDonald, P. R. LeBreton, and D. R. Herschback, Rev. Sci. Instrum. **40**, 1402 (1969); N. R. Daly, *ibid*. **31**, 264 (1960).
[14] S. W. North, D. A. Blank, P. M. Chu, and Y. T. Lee, J. Chem. Phys. **102**, 791 (1995).
[15] X. Zhao, Ph.D. thesis, University of California, Berkeley, 1989.
[16] *Handbook of Chemistry and Physics* (CRC Boca Raton, 1995).
[17] DMSO at 298 K contains ~2.3 kcal/mol of vibrational energy on average and should experience substantial cooling following supersonic expansion.
[18] R. N. Zare. Mol. Photochem. **4**, 1 (1972).
[19] R. D. Levine and R. B. Bernstein, Acc. Chem. Res. **7**, 393 (1974); J. T. Muckerman, J. Phys. Chem. **93**, 179 (1989).
[20] T. K. Minton, P. Felder, R. J. Brudzynski, and Y T. Lee, J. Chem. Phys. **81**, 1759 (1984); S. W. North, D. A. Blank, and Y. T. Lee, Chem. Phys. Lett. **222**, 38 (1994).
[21] R. N. Rudolph, S. W. North, G. E. Hall, and T. J. Sears (in preparation).
[22] P. M. Kroger and S. J. Riley, J. Chem. Phys. **67**, 4483 (1977); **70**, 3863 (1979).
[23] G. E. Hall, D. Vanden Bout, and T. J. Sears, J. Chem. Phys. **94**, 4182 (1991).